https://dx.doi.org/10.22161/ijaers.77.37 ISSN: 2349-6495(P) | 2456-1908(O)

The effect of shielding gases in the Ferrite Number of austenitic stainless steels joints through GMAW

André de Albuquerque Vicente[1,2], Peter Aloysius D'silva[2], Italo Leonardo dos Santos[2], Renato Rodrigues de Aguiar[2], Amilton Barbosa Botelho Junior[1], Tiago Felipe de Abreu Santos[3]

[1]Department of Chemical Engineering, Universidade de São Paulo, Rua do Lago,250, Cidade Universitária, São Paulo, SP, Brazil;
[2]ESAB Middle East & Africa,Plot No. S20134, Jebel Ali Free Zone (South), PO Box 8964, Dubai, United Arab Emirates;
[3]Department of Mechanical Engineering, Universidade Federal de Pernambuco, Av. da Arquitetura, s/n, Cidade Universitária, Recife, PE, Brazil.

Abstract *— In order to better understanding the effect of shielding gases in the volume fraction of δ ferrite in welded deposits through GMAW, the microstructures of four welded joints of austenitic stainless steel produced by the MIG/MAG process with different shielding gases were studied. The deposits were produced using the same welding electrode ER309Land welding parameters, but different shielding gases from pure argon to mixtures with increasing contents of CO_2. Each of the welding deposits were produced with 100% Ar, Ar+2% CO_2, Ar+4% CO_2 and Ar+20% CO_2. The chemical compositions and the variation of the volume fractions of δ ferrite in the deposits was measured. There was an increasing pickup of carbon and decreasing volume fraction of δ ferrite in the all weld metals produced using shielding gases with increasing concentrations of CO_2.The results confirm that carbon is a strong austenite stabilizer in austenitic stainless steels. Complementary techniques of microstructural analysis were used, such as optical emission spectrometry, optical microscopy and quantitative image analysis.*

Keywords *— **Austenitic Stainless Steels; Solidification Mode; Ferrite Number; GMAW.***

I. INTRODUCTION

In addition to iron, chromium and nickel, stainless steels have other chemical elements in their composition that can stabilize ferrite and austenite. Schaeffler **[1]** grouped these elements into two expressions called chromium equivalent and nickel equivalent, respectively, and proposed a diagram that is shown in Figure 1, considering the ferritizing and austenitizing effects of different alloying elements.

The Schaeffler diagram is not an equilibrium diagram. It was determined experimentally in order to predict the δ ferrite content in stainless steel welds.**[2,3]**

Creq =% Cr +% Mo + 1.5% Si + 0.5% Nb
(Equation 1)

Nieq =% Ni + 0.5% Mn + 30% C
(Equation 2)

In addition to the expressions of chromium and nickel equivalent proposed by Schaeffler, several other expressions have been suggested in the literature incorporating other elements, using other solidification conditions and different chemical compositions. **[2-11]**

In welding of high alloy steels, the δferrite content is normally estimated fromthe constitution diagrams such as the Schaeffler**[1]**, DeLong **[6]** and Kotechi**[11]**.

In these diagrams, the ferrite contents of various welds had been measured experimentally by either metallography (Schaeffler) or magnetic methods (DeLongand WRC–92).**[12]**

From the Schaeffler diagram, the first striking change was made by Delong **[6]**, which includes the austenitizing effect of nitrogen in the nickel equivalent formula and proposed a diagram that is shown in Figure 2.

https://dx.doi.org/10.22161/ijaers.77.37 *ISSN: 2349-6495(P) | 2456-1908(O)*

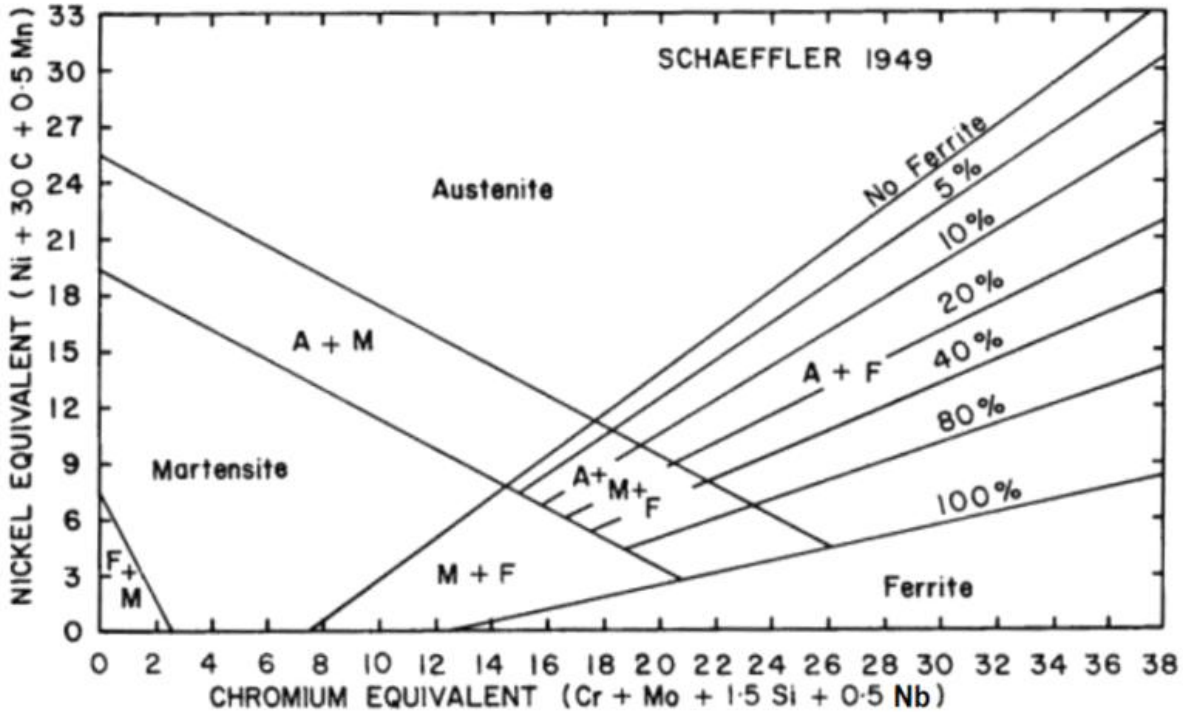

Fig.1: Schaeffler Diagram. [1]

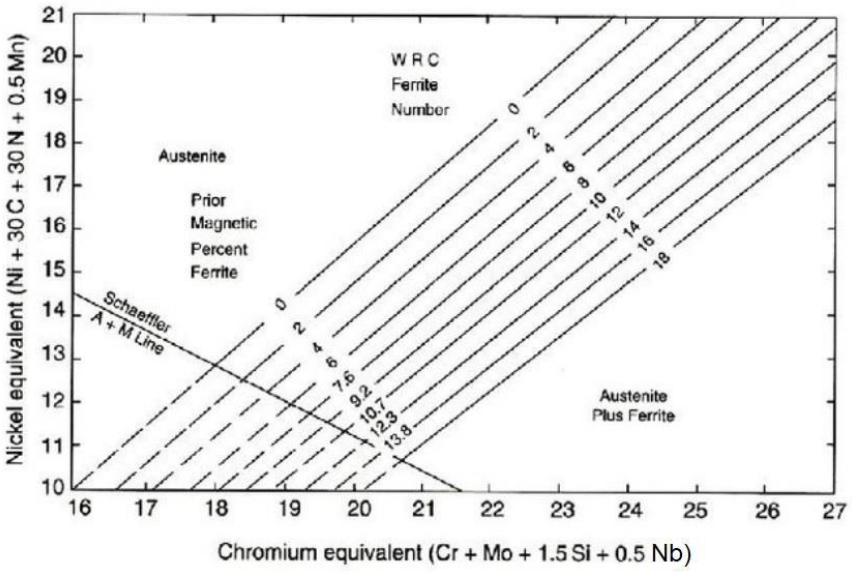

Fig.2: DeLong Diagram.[6]

O. Hammar and U. Svensson**[4]** showed that the addition of carbon and nitrogen decreases the volumetric fraction of ferrite in austenitic stainless steels.Taking as an example the austenitic stainless steel of type AISI 316, which usually solidifies through a ferritic-austenitic solidification mode. With the increasing of carbon and nitrogen contents as alloying elements, the solidification mode changes to austenitic-ferritic. There is, therefore, acarbon equivalent value that can change how this steel solidifies.

Ceq =% C + 0.65% N

(Equation 3)

Figure 3 shows the variation of the volume fraction of primary δ ferrite as a function of carbon equivalent.

https://dx.doi.org/10.22161/ijaers.77.37 *ISSN: 2349-6495(P) | 2456-1908(O)*

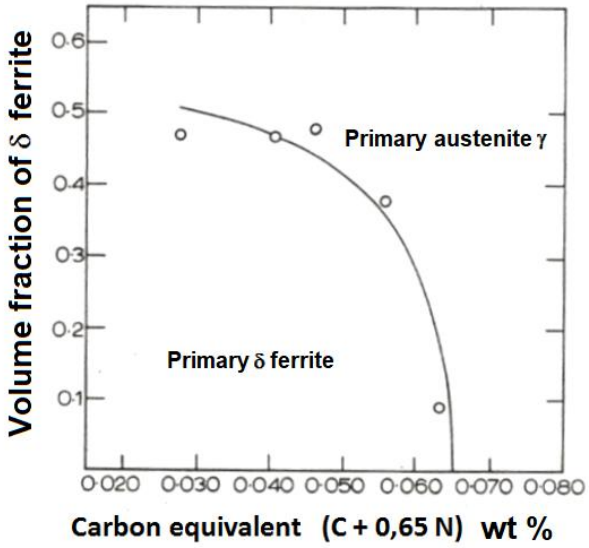

Fig.3: Volume fraction of δ ferrite as a function of C_{eq}. [2,4]

The WRC – 92 diagram estimates the ferrite content to reasonably good accuracy and also provides additional information aboutthe solidification mode as shown on figure 4.**[12]**

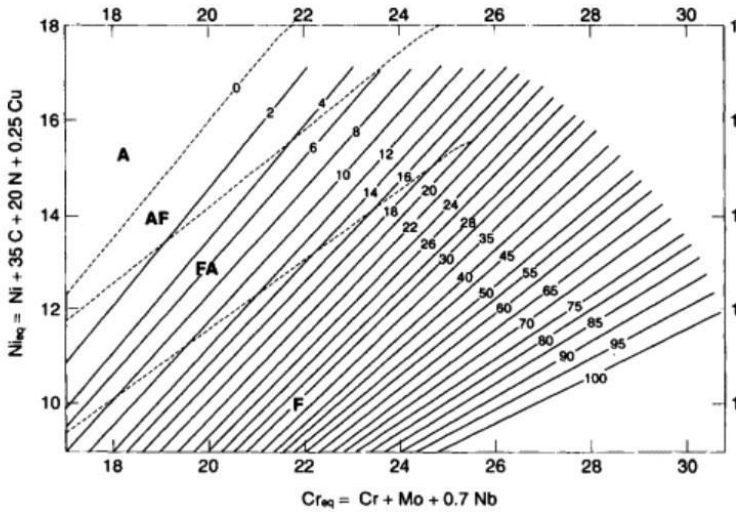

Fig.4: WRC-92 Diagram.[11]

Kotechi**[11]** has pointed out that there are number of alloying elements that have not been considered in the most accurate diagram to date, the WRC – 92 diagram. Elements like silicon, titanium, tungsten are not given due considerations though they are known to influence the ferrite content. He also stressed the point that cooling rate effects need to be considered more thoroughly in these constitution diagrams.**[12]**

Table1 shows the expressions of chromium and nickel equivalents proposed by Schaeffler**[1]**, DeLong **[6]** and Kotechi**[11]**.

Table 1 -Cr_{eq} and Ni_{eq} formulae used for estimating the delta-ferrite content from constitution diagrams[12]

Consitution Diagram	
Schaeffler Diagram (1949)	Cr_{eq} = Cr + Mo + 1.5xSi + 0.5xNb
	Ni_{eq} = Ni + 30xC + 0.5xMn
DeLong Diagram (1973)	Cr_{eq} = Cr + Mo + 1.5xSi + 0.5xNb
	Ni_{eq} = Ni + 30xC + 30xN + 0.5xMn
WRC-92 Diagram (1992)	Cr_{eq} = Cr + Mo + 0.7xNb
	Ni_{eq} = Ni + 35xC + 20xN + 0.25xCu

When the Cr_{eq}/Ni_{eq} ratio <1.5, the solidification may be austenitic (mode I) or austenitic-ferritic (mode II). When the ratio 1.5 <Cr_{eq}/Ni_{eq}<2.0 the solidification will be ferritic-austenitic (mode III). And finally, when Cr_{eq}/Ni_{eq}ratio > 2.0 the solidification will be ferritic (mode IV).**[2,3,13-15]**

The possible solidification modes in the Fe-Cr-Ni system are:

I) ***Austenitic solidification (L→L+γ→γ):***
The only solid phase to form is austenite. In austenitic solidification, called solidification mode I, there is no other phase transformation at high temperature.**[2-3]**

II) **Austenitic-ferritic solidification *(L →L+γ→ L+γ+δ→γ+δ):***

https://dx.doi.org/10.22161/ijaers.77.37 *ISSN: 2349-6495(P) | 2456-1908(O)*

Austenite solidifies as a primary phase in a dendritic or cellular way. As the temperature decreases, ferrite δ is formed from the remaining liquid. Solidification occurs through a peritectic reaction (L+δ→γ). This is called solidification mode II. **[13-15]**

III) ***Ferritic-austenitic solidification (L→L+δ→L+δ+γ→δ+γ):***

The duplex stainless steels solidify according to ferritic-austenitic solidification (L→L+δ→L+δ+γ→δ+γ). δ ferrite solidifies as the primary phase in dendritic or cellular fashion. As temperature decreases, austenite is formed by a peritectic (L+δ→γ) or eutectic (L→δ+γ) reaction. In the case of a peritectic reaction, the initially formed austenite completely surrounds the ferrite and subsequently grows into ferrite and liquid. Depending on the rate of diffusion through the austenite, the reaction may or may not be complete, and at the end of the solidification ferrite may be involved in austenite. Between the two reactions - peritectic and eutectic - the transition takes place where, during the initial formation of austenite by peritectic reaction, ferritizing elements secrete to the liquid, provoking their enrichment in these elements and consequently the simultaneous formation of ferrite and austenite by means of a eutectic reaction. This is called solidification mode III.**[13-21]**

IV) ***Ferritic solidification (L→L+δ→δ):***

The only solid phase to form is ferrite. In ferritic solidification, called solidification mode IV, ferrite is the only phase to form during solidification and, depending on the chemical composition, austenite can precipitate only in the solid state in the ferritic grain boundaries.**[2,3]**

The solidifications of austenitic stainless steels can occur according to the first three solidification modes. Depending on the conditions of solidification, the factors for the elements in the expressions of chromium and nickel can vary widely and some elements that do not influence the expressions, depending on the process, can be important when dealing with different solidification modes.

Table 2 shows the expressions of chromium and nickel equivalents suggested by different researchers, considering different production process of stainless steels.

Table.2: Expressions of Cr_{eq} and Ni_{eq} suggested by different researchers. [2, 19]

Author		**Schaeffler**	**DeLong**	**Pryce e Andrews (1)**	**Giraldeng**	**Potak e Sagalevich apud Hull**	**Hull (2)**	**Hammar e Svensson**
Production Process		**Welding**	**Welding**	**Hot Rolling**	**Casting**	**Casting**	**Gravity Casting**	**Thermal Analysis**
Ferritiziting Alloying Elements	**Cr**	1,00	1,00	1,00	1,00	1,00	1,00	1,00
	Mo	1,00	1,00	1,00	2,00	1,00	1,21	1,37
	Si	1,50	1,50	3,00	1,50	2,00	0,48	1,50
	Nb	0,50	0,50	4 Nb'	-	0,90	0,14	2,00
	Ti	-	-	10 Ti'	4,00	4,00	2,20	3,00
	W	-	-	-	-	0,50	0,72	-
	V	-	-	-	-	1,50	2,27	-
	Al	-	-	-	3,00	4,00	2,48	-
	Ta	-	-	-	-	-	0,21	-
Austenitizing Alloying Elements	**Ni**	1,00	1,00	1,00	1,00	1,00	1,00	1,00
	Mn	0,50	0,50	0,50	-	0,50	Mn'	0,31
	C	30,00	30,00	21,00	30,00	27,00	24,50	22,00
	N	-	30,00	11,50	20,00	27,00	18,40	14,20

https://dx.doi.org/10.22161/ijaers.77.37 *ISSN: 2349-6495(P) | 2456-1908(O)*

	Cu	-	-	0,44	-	0,33	0,44	1,00
	Co	-	-	-	-	0,40	0,41	-

(1) Nb' = Nb – 8x[(C-0,03)+N] and Ti' = Ti – 4x[(C-0,03)+N]

(2) Mn' = 0,11xMn - 0,0086xMn^2

II. EXPERIMENTAL

Four welded joints of austenitic stainless steel produced by the MIG/MAG process with different shielding gases were studied. The deposits were produced using the same welding electrode ER309L1,2 mm according to AWS 5.9, and welding parameters, but different shielding gases from pure argon to mixtures with increasing contents of CO_2. Each of the welding deposits were called sample 1, sample 2, sample 3 and sample 4 and produced, respectively,using100% Ar, Ar+2% CO_2, Ar+4% CO_2 and Ar+20% CO_2, as the shielding gases. The GMAWwelding machine was adjusted to allow a stable welding for the four shielding gases.

After adjustment of optimum welding parameters to have arc stability with the different shielding gases, an automatic welding tractor was used to guarantee the correct travel speeds to have similar heat inputs for all the four samples.

In order to minimize the effect of base metal chemical composition, 6 layers of 5 beads each were deposited.Overlapping passes were used, depositing approximately 25 mm on the base metal that was an AISI 304L type stainless steel.The weld pads were cut in longitudinal and transversal directions. Chemical analyzes were carried out in all samples at 20 mm from the base metal, by means of an optical emission spectrometer, according to ASTM E 1086-08. **[22]**

Afterwards, the samples transversal and longitudinal samples were embedded in hot-cure resin (bakelite). The conventional manual polishing was applied using water slicks (100, 240, 320, 400, 600 and 1000 mesh) in order to standardize the surface finish of the samples. A cloth polishing with 9, 3 and 1 μm diamond abrasive paste was carried out in this sequence. The samples were electrolytically attacked in 20% NaOH solution, 6V, for 90 seconds. This allowed the microstructural characterization of the samples through optical microscopy. The quantitative metallographic analysis for the determination of volumetric fractions of δ ferrite and austenite were performed according to ASTM E 562 ed. 08, **[23]** using a 4X5 grid (20 points) with a magnification of 400X in 30 different regions per test piece.

III. RESULTS AND DISCUSSION

Table 3 presents the welding parameters used to weld the samples.It is important to emphasize that the welding wire used to produce samples 1, 2, 3 and 4 wasthe ER309L according to AWS 5.9, 1.2 mm diameter.

Table.3: Welding parameters.

	Shielding gas	**Flow (l/min)**	**Current (A)**	**Tension (V)**	**Driving Speed (mm/min)**	**Heat Input (kJ/mm)**
Sample 1	Ar	20	199	26	230	1.35
Sample2	Ar + 2% CO_2	20	216	27	261	1.34
Sample 3	Ar + 4% CO_2	20	210	26	243	1.35
Sample 4	Ar + 20% CO_2	20	200	27	237	1.37

Table 4 presents the chemical compositions and the calculations of C_{eq}, according to O. Hammar and U. Svensson**[4],** of the filler metal and the all weld metals of the four joints. It is important to emphasize thatthe chemical analyzes were carried out in all samples at 20 mm from the base metal.

The calculations of C_{eq} were done using **Equation 3**.

https://dx.doi.org/10.22161/ijaers.77.37 *ISSN: 2349-6495(P) | 2456-1908(O)*

Table.4: Chemical compositions and the calculations of C_{eq},

	C	Si	Mn	P	S	Cr	Ni	Mo	Cu	N	C_{eq}
309L	0.017	0.48	1.77	0.016	0.015	24.23	12.91	0.05	0.06	0.071	**0.063**
Sample 1	0.014	0.46	1.69	0.016	0.015	23.33	13.09	0.05	0.06	0.072	**0.061**
Sample 2	0.017	0.44	1.62	0.016	0.015	23.30	13.11	0.05	0.05	0.069	**0.062**
Sample 3	0.018	0.42	1.55	0.016	0.015	23.30	13.10	0.05	0.05	0.068	**0.062**
Sample 4	0.023	0.41	1.52	0.016	0.015	23.23	13.11	0.05	0.05	0.068	**0.067**

Table 5 presents the calculated values Cr_{eq},Ni_{eq} and Cr_{eq}/Ni_{eq} ratio according to the expressions of chromium and nickel equivalents proposed by Schaeffler**[1]**, DeLong **[6]** and Kotechi**[11]**. The calculations of Cr_{eq},Ni_{eq} and Cr_{eq}/Ni_{eq} ratio were done using formulas taken from Table 1.

Table.5: Cr_{eq}, Ni_{eq} and Cr_{eq}/Ni_{eq} ratio according to the expressions of chromium and nickel equivalents proposed by Schaeffler, DeLongand Kotechi.

	Schaeffler Diagram (1949)			DeLong Diagram (1973)			WRC-92 Diagram (1992)		
	Cr_{eq}	Ni_{eq}	Cr_{eq}/Ni_{eq}	Cr_{eq}	Ni_{eq}	Cr_{eq}/Ni_{eq}	Cr_{eq}	Ni_{eq}	Cr_{eq}/Ni_{eq}
309L	24.95	14.31	**1.74**	24.95	16.43	**1.52**	24.28	14.94	**1.63**
Sample 1	24.01	14.38	**1.67**	24.01	16.53	**1.45**	23.38	15.06	**1.55**
Sample 2	23.96	14.44	**1.66**	23.96	16.52	**1.45**	23.35	15.12	**1.54**
Sample 3	23.93	14.41	**1.66**	23.93	16.44	**1.46**	23.35	15.10	**1,55**
Sample 4	23.85	14.57	**1.64**	23.85	16.60	**1.44**	23.28	15.29	**1.52**

The results presented on table 4 and 5, show that increasing the concentration of CO_2 in the shielding gases increases the concentration of C in the deposited metal. The results obtained suggest that with an increase in the concentration of CO_2 in the shielding gases, a decrease in the Cr_{eq} of the alloys occurs due to the selective oxidation of the elements Cr and Si.
Figure 5 shows the contents of C, Si, Mn and Cr (% by weight) of filler metal ER 309L and welded chemical pads.

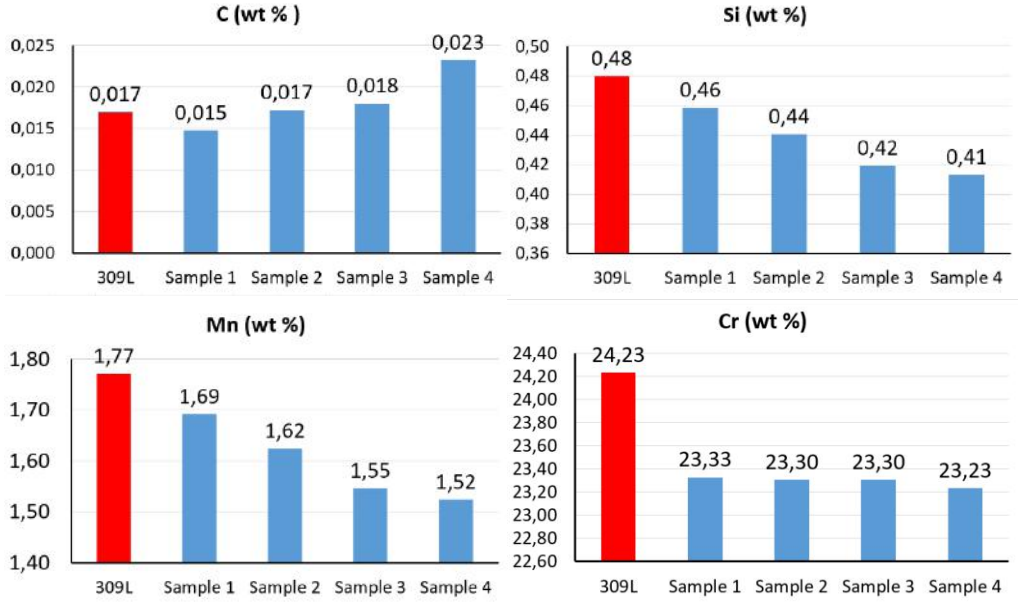

Fig.5: Contents of C, Si, Mn and Cr (% by weight) of filler metal ER 309L and chemical pads welded.

https://dx.doi.org/10.22161/ijaers.77.37 *ISSN: 2349-6495(P) | 2456-1908(O)*

Despite the selective oxidation of Mn, the observed trend is of increasing of the Ni_{eq}.
Figure 6 shows the variations of the Cr_{eq} and Ni_{eq} values (% by weight) and the Cr_{eq}/Ni_{eq} ratio of the filler metal ER 309L and the welded chemical pads according to the expressions of chromium and nickel equivalents proposed by Schaeffler, DeLongand Kotechi.

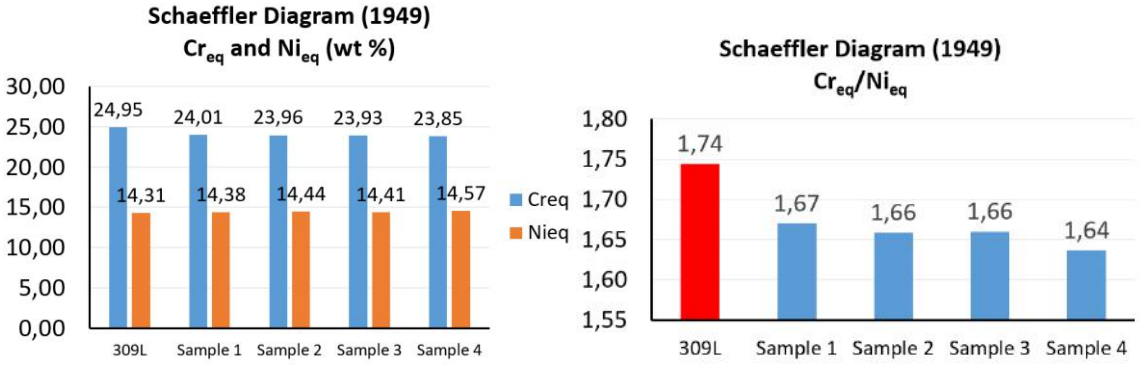

a)

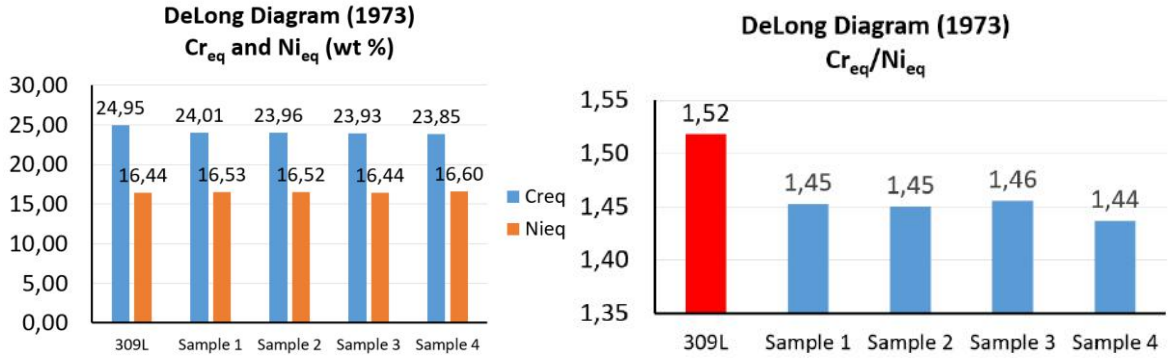

b)

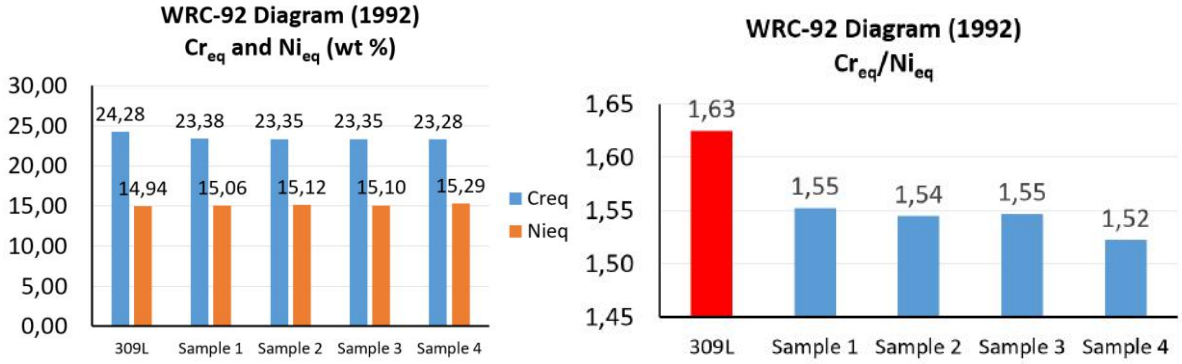

C)

Fig.6: Cr_{eq} and Ni_{eq} values (% by weight) and the Cr_{eq}/Ni_{eq} ratio of the filler metal ER 309L and the welded chemical pads according to the expressions of chromium and nickel equivalents proposed by:a) Schaeffler, b) DeLongand c) Kotechi.

https://dx.doi.org/10.22161/ijaers.77.37 *ISSN: 2349-6495(P) | 2456-1908(O)*

Table 6 presents the volume fractions of δ ferrite measured through metallographic analysis in 30 different regions per test piece.

Table.6: Volume fractions of δ ferrite measured optical microscopy.

Volume fraction of δ ferrite	Mean	95%CI	%RA
Sample 1 Transversal	13,1	1,5	13,6
Sample 1 Longitudinal	10,4	1,7	16,2
Sample 1 - Average	**11,2**	**1,8**	**17,6**
Sample 2 Transversal	12,6	1,3	13,3
Sample 2 Longitudinal	9,5	1,2	11,2
Sample 2 - Average	**10,7**	**1,6**	**18,6**
Sample 3 Transversal	11,5	1,5	18,5
Sample 3 Longitudinal	8,7	1,3	11,2
Sample 3 - Average	**10,4**	**1,5**	**17,3**
Sample 4 Transversal	10,9	0,9	13,2
Sample 4 Longitudinal	8,3	1,2	12,6
Sample 4 - Average	**9,9**	**1,6**	**19,3**

Figure 7 shows the micrographs obtained approximately 20 mm from the base metal in the transversal direction of the welded specimens.

Metallographic analysis revealed austenitic-ferritic microstructures for all welded specimens, with austenite being the light phase and ferrite being the dark phase in the grain boundaries.

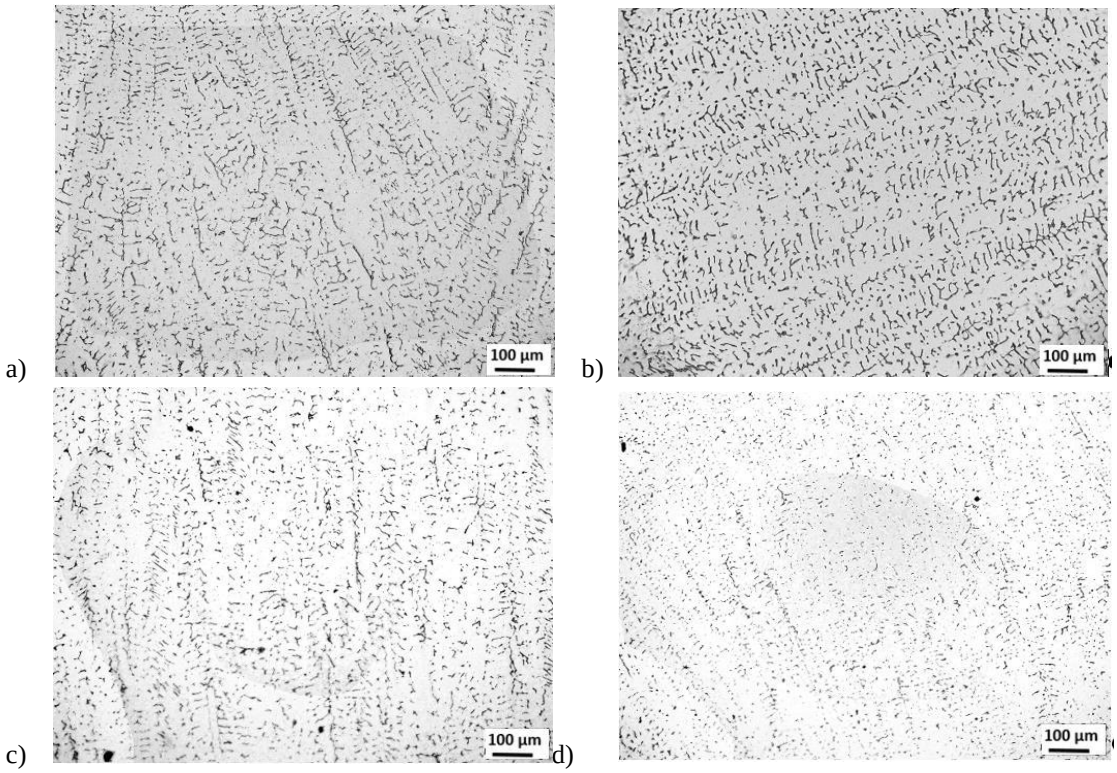

Fig.7: Cross-sectional micrographs of welded specimens.a) Sample 1, b) Sample 2, c) Sample 3 and d) Sample 4.Electrolytic attack with 20% NaOH with 6.5 V for 1.5 minutes.

https://dx.doi.org/10.22161/ijaers.77.37 *ISSN: 2349-6495(P) | 2456-1908(O)*

The volumetric fractions of δ ferrite verified in the longitudinal direction are smaller than those verified for the transversal direction in the four welded specimens.

The metallographic analysis of the welded specimens revealed that the increase in the concentration of CO_2 in the shielding gases decreases the volume fraction of δ ferrite in the deposited metal.

As discussed earlier, these results are consistent with chemical analysis of chemical weld pads. In Figure 6, it can be seen, that with the increase of the CO_2 concentration in the shielding gases, there is a decrease in Cr_{eq} and an increase in Ni_{eq}, resulting in a decrease in the Creq / Nieq ratio of the alloys.

IV. CONCLUSIONS

The increase in the concentration of CO_2 in shielding gases increases the $Ni_{eq}$of the alloys by increasing thecontent of carbon in the deposited all weld metal.

The results obtained suggest that increasing the concentration of CO_2 in the shielding gases decreases in the Cr_{eq} of the alloys due to the selective oxidation ofCr and Si elements.

Increasing the carbon content of the alloy decreases the volume fraction of δ ferrite in the deposited all weld metal.

The results obtained suggest that solidification of the studied alloys is ferritic-austenitic (mode III).

The increase in concentration of CO_2 in shielding gases decreases Cr_{eq} and increase Ni_{eq}, in the deposited all weld metal, resulting in the decrease in the Cr_{eq}/Ni_{eq} ratio of the alloys.

REFERENCES

[1] SCHAEFFLER, A. L..**Constitution diagram for stainless steel weld metal**. Metal Progress, vol. 56, n.5, p. 680-680B, 1949.

[2] Vicente, A. A.. **Estudo da resistência à oxidação ao ar a altas temperaturas de um aço inoxidável austenítico microligado ao cério soldado pelo processo mig/mag com diferentes gases de proteção.** Tese de Doutorado, Escola Politécnica, Universidade de São Paulo, São Paulo. 2017. https://doi:10.11606/T.3.2017.tde-05092017-103140.

[3] Sindo Kou, **"Welding metallurgy"**, John Wiley & Sons, Inc., 2003, USA.ISBN:9780471434023.

[4] HAMMAR, O.; SVENSSON, U..**Influence of Steel Composition on Segregation and Microstructure During Solidification of Austenitic Stainless Steels.** Solidification and Casting Metals, London, Metals Society, p. 401- 410, 1979.

[5] SUUTALA, N.; **TAKALO**, T.; MOISIO, T.. **Ferritic-Austenitic Solidification mode in Austenitic Stainless Welds.**Metalurgical Transactions A, vol 11A, p. 717-725, 1980.

[6] DeLONG, W. T..**A modified phase diagram for stainless steel weld metals.**Metal Progress, p. 98-100B, 1960.

[7] SUUTALA, N.; MOISIO, T..**Use of chromium and nickel equivalents in considering solidification mode in austenitic stainless steel welds.**Solidification and Casting Metals, London, The Metals Society, p. 310- 314, 1979.

[8] SUUTALA, N.; TAKALO, T.; MOISIO, T.. **The relationship between solidification and microstructure in austenitic-ferritic stainless steel welds.**Metallurgical Transactions A, vol. 10A, p.512-514, 1979.

[9] TAKALO, T.; SUUTALA, N.; et al..**Austenitic solidification mode in austenitic stainless steel welds.**Metallurgical Transactions A, vol. 10A, p. 1173-1181, 1979.

[10] SUUTALA, N.; TAKALO, T.; et al..**Single-phase ferritic solidification mode in austenitic-ferritic stainless steel welds.**Metallurgical Transactions A, vol. 10A, p. 1183-1190, 1979.

[11] D.J. KOTECHI; D. T.A. SIEWERT. **WRC – 92 Constitution Diagram for Stainless Steel Weld Metals: a Modification of the WRC – 1988 Diagram**. Welding Journal 71 (5), 171–178, 1992.

[12] M. Vasudevan, M. Murugananth, A.K. Bhaduri, **Application of Bayesian neural network for modeling and prediction of FN in austenitic stainless steel welds**, in: H. Cerjak, H.K.D.H. Bhadeshia (Eds.), Mathematical Modelling of Weld Phenomena—VI, Institute of Materials, 2002, pp. 1079–1099.

[13] VICENTE, A. A.; D'SILVA, P. A.; SOUZA, R. L.; SANTOS, I. L.; AGUIAR, R. R.; JUNIOR, A. B. B..**The use of duplex stainless steel filler metals to avoid hot cracking in GTAW welding of austenitic stainless steel AISI 316L.**International Journal of Advanced Engineering Research and Science, 7(6), pp.345-355, 2020. https://doi.org/10.22161/ijaers.76.43.

[14] VICENTE, A. A.; SOUZA, R. L.; ESPINOSA, D. C. R.; AGUIAR, R. R.; PAUL, P.;. **Effect of relative plate thickness in the heat flow and cooling rate during welding of super duplex stainless steel.** Saudi Journal of Engineering and Technology, 5 (5), 244-150. Scholars Middle East Publishers, Dubai, United Arab Emirates, 2020.https://doi.org/10.36348/sjet.2020.v05i05.005.

[15] VICENTE, A. A.; SANTOS, I. L.; JUNIOR, A. B. B.; ESPINOSA, D. C. R.; TENÓRIO, J. A. S..**Study of the Distribution of Cr, Mo, Ni and N in δ Ferrite and Austenite in Duplex Stainless Steels**.Saudi Journal of Engineering and Technology, 5 (4), 156-162. Scholars Middle East Publishers, Dubai, United Arab Emirates, 2020.https://doi.org/10.36348/sjet.2020.v05i04.005.

[16] Santa-Cruz, L.A., Machado, G., Vicente, A.A. et al. **Effect of high anodic polarization on the passive layer properties of superduplex stainless steel friction stir welds at different chloride electrolyte pH values and temperatures.**Int J Miner Metall Mater 26, 710–721 (2019). https://doi.org/10.1007/s12613-019-1790-0.

[17] MARQUES, Igor Jordão; VICENTE, André de Albuquerque; TENORIO, Jorge Alberto Soares and

https://dx.doi.org/10.22161/ijaers.77.37 *ISSN: 2349-6495(P) | 2456-1908(O)*

SANTOS, Tiago Felipe de Abreu. **Double Kinetics of Intermetallic Phase Precipitation in UNS S32205 Duplex Stainless Steels Submitted to Isothermal Heat Treatment.** Materials Research, 20(Suppl. 2), 152-158. Epub June 26, 2017. https://doi.org/10.1590/1980-5373-mr-2016-1060.

[18] A. de Albuquerque Vicente, J.R.S. Moreno, D.C.R. Espinosa,T.F. de Abreu Santos, J.A.S. Tenório. **Study of the high temperature oxidation and Kirkendall porosity in dissimilar welding joints between FE-CR-AL alloy and stainless steel AISI 310 after isothermal heat treatment at1150 °C in air.** J. Mater. Res. Technol. 8(2), 1636 (2019).https://doi.org/10.1016/j.jmrt.2018.11.009.

[19] Vicente, A. A.; Cabral, D. A.; Espinosa, D. C. R.; Tenório, J. A. S.. **Efeito dos gases de proteção na microestrutura e nas cinéticas de oxidação a altas temperaturas ao ar de juntas soldadas de um aço inoxidável austenítico através do processo MIG/MAG.** Tecnol. Metal. Mater. Min., vol.14, n4, p.357-365, 2017. https://doi.org/10.4322/2176-1523.1264.

[20] MARQUES, Igor Jordão; SILVA, Flavio J.; SANTOS, Tiago Felipe de Abreu. **Rapid precipitation of intermetallic phases during isothermal treatment of duplex stainless steel joints produced by friction stir welding.** Journal of Alloys and Compounds, Volume 820, 2020. https://doi.org/10.1016/j.jallcom.2019.153170.

[21] Santa Cruz, L.A., Marques, I.J., Urtiga Filho, S.L.et al.**Corrosion Evaluation of Duplex and Superduplex Stainless Steel Friction Stir Welds Using Potentiodynamic Measurements and Immersion Tests in Chloride Environments.**Metallogr. Microstruct. Anal.8,32–44 (2019). https://doi.org/10.1007/s13632-018-0506-6.

[22] ASTM E1086-08: Standard Test Method for Optical Emission Vacuum Spectrometric Analysis of Stainless Steel by the Point-to-Plane Excitation Technique. ASTM International. West Conshohocken. PA. EUA. 2008.

[23] ASTM E562-08: Standard Test Method for Determining Volume Fraction by Systematic Manual Point Count. ASTM International. West Conshohocken. PA. EUA. 2008.